ACS APPLIED MATERIALS & INTERFACES

Research Article

www.acsami.org

Low-Temperature Fabrication of Mesoporous Titanium Dioxide Thin Films with Tunable Refractive Indices for One-Dimensional Photonic Crystals and Sensors on Rigid and Flexible Substrates

Cheng Li, Nicholas S. Colella, and James J. Watkins*

Department of Polymer Science and Engineering, University of Massachusetts—Amherst, 120 Governors Drive, Amherst, Massachusetts 01003, United States

Supporting Information

ABSTRACT: Highly transparent mesoporous titanium dioxide (TiO_2; anatase) thin films were prepared at room temperature via ultraviolet (UV) irradiation of hybrid polymer−TiO_2 nanoparticle thin films. This approach utilized a UV-curable polymer in conjunction with the photocatalytic activity of TiO_2 to form and degrade the organic component of the composite films in one step, producing films with well-controlled porosity and refractive index. By adjustment of the loading of TiO_2 nanoparticles in the host polymer, the refractive index was tuned between 1.53 and 1.73. Facile control of these properties and mild processing conditions was leveraged to fabricate robust one-dimensional photonic crystals (Bragg mirrors) consisting entirely of TiO_2 on silicon and flexible poly(ethylene terephthalate) substrates. The mesoporous Bragg mirrors were shown to be effective chemical vapor sensors with strong optical responses.

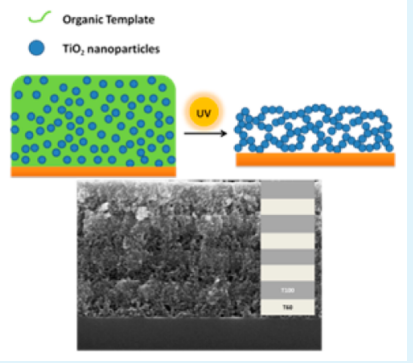

KEYWORDS: *UV treatment, mesoporous films, Bragg mirrors, flexible substrate*

INTRODUCTION

Bragg mirrors, structures made from alternating layers of two different dielectric materials, are common optical components used in many applications such as lasers,[1,2] light-emitting diodes,[3,4] and solar cells.[5,6] They are employed because of their strong reflectance at a well-defined wavelength range, which results from constructive interference of reflected light at the interface between each layer. The intensity, wavelength, and bandwidth of the reflected light are determined by the refractive index, thickness, and number of layers. For manufacturing, thin-film deposition techniques such as physical vapor deposition[7] and chemical vapor deposition[8] are employed to achieve highly uniform films and finely controlled film thicknesses. Combined with sol−gel methods, solution-based deposition techniques such as spin coating[9,10] and dip coating[11,12] are also employed to fabricate Bragg mirrors over large areas. Bragg mirrors made from the self-assembly of block copolymer gels and bottlebrush block copolymers have also been reported.[13−15]

Recently, the use of porous materials as building blocks for Bragg mirrors has attracted significant attention.[16,17,21,22] Optical responses arising from chemical and biological stimuli provide novel applications for mesoporous Bragg mirrors as sensors and detectors.[23] One way to obtain mesoporous thin-film materials is to use sol−gel precursors combined with surfactants or block copolymers as templates.[16−20] Typically, mesoporous titanium dioxide (TiO_2) and silicon oxide (SiO_2) with Pluronics and cetrimonium bromide templates are employed because the resulting materials have sufficient refractive index contrast to provide a strong and well-defined reflectance waveband.[16] After high-temperature calcination, ordered and interconnected mesoporous structures are generated within each layer. The absorption of target compounds modifies the refractive index of each mesoporous layer, resulting in an altered optical response. Selective responses to specific compounds can be realized by chemical functionalization of the pore surfaces, enabling the concept of a "Photonic nose".[17,23] Porous Bragg mirrors can also be made from a single material, where the refractive index contrast results from a porosity difference between layers. In one example, poly(isoprene-*block*-ethylene oxide) was employed as a template of TiO_2 sol−gel precursors.[22] However, high-temperature calcination above 500 °C was necessary to crystallize the amorphous TiO_2 phase templated by the polymer, which limits the application of the materials on flexible substrates such as poly(ethylene terephthalate) (PET).

An alternative way to achieve mesoporous Bragg mirrors is to use crystalline nanoparticle films as building blocks. Spin-coating[24] and layer-by-layer deposition[25] are commonly employed. Compared with the template-directed sol−gel methods, the nanoparticle route is usually less time-consuming and more robust. TiO_2 and SiO_2 nanoparticles are commonly used because they have a large refractive index contrast (bulk TiO_2 = 2.49; bulk SiO_2 = 1.45). Many other nanoparticles have also been synthesized and employed as building blocks for

Received: September 23, 2014
Accepted: May 29, 2015
Published: May 29, 2015

DOI: 10.1021/acsami.5b03240
ACS Appl. Mater. Interfaces 2015, 7, 13180−13188

mesoporous Bragg mirrors including ZrO_2,[26] Fe_2O_3,[27] ZnO,[27] and NiO and WO_3.[28] The diversity of the nanoparticles provides Bragg mirrors with novel properties and applications such as selective UV reflecting mirrors[26] and electrochromic Bragg mirrors[28] as a means to enhance the efficiency of photovoltaic devices.[29−32]

Here we present a rapid and low-cost method for fabricating highly transparent mesoporous TiO_2 thin films with tunable porosity at room temperature on either silicon or plastic substrates by exploiting the photocatalytic properties of TiO_2. Anatase TiO_2 is a well-known photocatalyst capable of degrading organic materials under UV light.[33] Additionally, recent research has focused on the effects of UV treatment on the electrochemical properties of TiO_2 films because UV irradiation provides a low-temperature sintering alternate to calcination, enabling device fabrication on flexible plastic substrates.[34−37] In our work, highly transparent hybrid TiO_2 nanocomposite films were obtained by dispersing TiO_2 nanoparticles in polymer templates. The porosity was tuned by controlling the loading of TiO_2 nanoparticles into hybrid films prior to UV irradiation, which results in a tunable refractive index. The mesoporous TiO_2 films were characterized by ellipsometry, IR spectroscopy, and scanning electron microscopy (SEM). By deposition of two TiO_2 hybrid films with precisely designed thicknesses and refractive indices, we generated porous TiO_2 Bragg mirrors with strong and well-defined reflections after UV irradiation. The Bragg mirror was optically sensitive to the adsorption of chemical vapors. Because of low-temperature fabrication, this method is compatible with flexible substrates such as PET.

EXPERIMENTAL SECTION

Materials. Titanium dioxide (TiO_2, anatase phase; 15 wt %) nanoparticles dispersed in water were purchased from Nanostructured & Amorphous Materials, Inc.; Norland Optical Adhesive 65 (NOA65) was purchased from Norland Products, Inc.; poly(acrylic acid) (PAA; M_w = 1800 g) and *N*-methyl-2-pyrrolidone (NMP; ReagentPlus 99%) were purchased from Sigma-Aldrich; methanol (MeOH) was purchased from Fisher Scientific; poly(ethylene terephthalate) (PET) films were purchased from Dupont; silicon wafers of (100) orientation (p-type, boron dopant) were purchased from NovaElectronics. All materials were used as received without further purification.

Solvent Exchange of TiO_2 Nanoparticle Dispersion. A 250 mL glass bottle with a screw cap was charged with 100 g of a 15 wt % water dispersion of TiO_2 nanoparticles. A total of 50 g of NMP and 50 g of MeOH were added to the TiO_2 dispersion and stirred. Then the solution was slowly dried under a constant air flow for 2 days until most of the water was removed. The obtained nanoparticle slurry was then redispersed by vortexing and sonicating using a Qsonica sonicator. The resulting dispersion had a TiO_2 concentration of approximately 15.3 wt %. The organic-solvent-based TiO_2 dispersions were stable for several months.

Preparation of Hybrid TiO_2 Nanocomposite Films and Photodegradation. Solutions of solvent-exchanged nanoparticles, additional NMP/MeOH solvent, and either PAA or NOA65 were prepared at the desired compositions. The solutions were then sonicated for 5 min with a Qsonica sonicator prior to spin coating. Silicon, glass, and PET substrates were used in spin coating. Spin coating was performed until the color of the films remained constant. The films were then put on a 60 °C hot plate for 15 min to evaporate the residual solvent. The TiO_2/NOA65 hybrid films were cured under a Xenon Corp. RC-500 pulsed UV curing system with a dose of 8 J/cm^2. Then the hybrid films were exposed to 264 nm UV with 4.5 mW/cm^2 for different periods of time at room temperature or at 65 °C to degrade the organic components. The obtained films were labeled as T100, T90, T80, T70, and T60. The number indicates the weight percent of TiO_2 nanoparticles in the hybrid films before UV irradiation.

Bragg Mirror Fabrication. A layer of TiO_2 hybrid film containing 60 wt % TiO_2 and 40 wt % NOA65 was formed by spin-coating. After complete degradation of the organic components under UV irradiation, a layer of TiO_2 nanoparticles was spin-coated on top. Then the previous two steps were repeated until the target number of layers was obtained. The substrate can be a silicon wafer or PET.

Characterization. Refractive indices and film thicknesses were characterized by a Sopra GES-5 variable-angle spectroscopic ellipsometer (VASE). Modeling of the VASE data was performed with *Winelli* commercial software available from Sopra. IR spectroscopic measurements were performed using a Bruker Vertex 70 Fourier transform infrared (FTIR) spectrophotometer in ATR mode. Transmittance UV−vis−near-IR spectroscopy was performed on a Shimadzu UV-3600 spectrophotometer. Reflectance measurements were conducted on a F20 spectrum reflectance instrument from Filmetrics. The relative humidity was 13% and the temperature was 20 °C in each of the solvent vapor tests. Field-emission scanning electron microscopy (FESEM) was performed on a FEI Magellan Field-emission scanning electron microscope.

RESULTS AND DISCUSSION

To obtain transparent and uniform porous TiO_2 nanoparticle films after UV degradation, aggregation between TiO_2 nanoparticles must be minimized in the hybrid films before irradiation. The organic templates or binders should be compatible with the nanoparticles and should not induce nanoparticle precipitation or aggregation in the solutions or thin films. The TiO_2 nanoparticles used in our experiments were initially well-dispersed in water. Unfortunately, the majority of polymers, oligomers, and monomers of interest for hybrid film formation are not soluble in water. To allow for more organic template options, a solvent exchange method was employed[38] (see the Experimental Section). The resulting solvent is a mixture of the polar aprotic solvent NMP and the

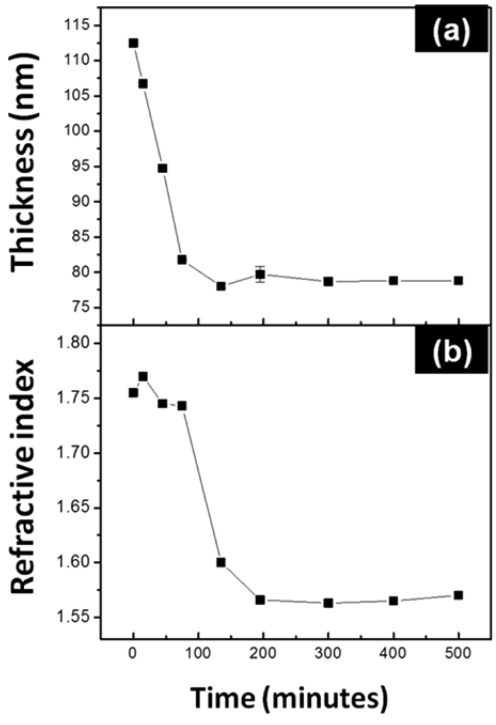

Figure 1. Thickness (a) and refractive index (b) changes of a TiO_2 hybrid film during UV irradiation.

DOI: 10.1021/acsami.5b03240
ACS Appl. Mater. Interfaces 2015, 7, 13180−13188

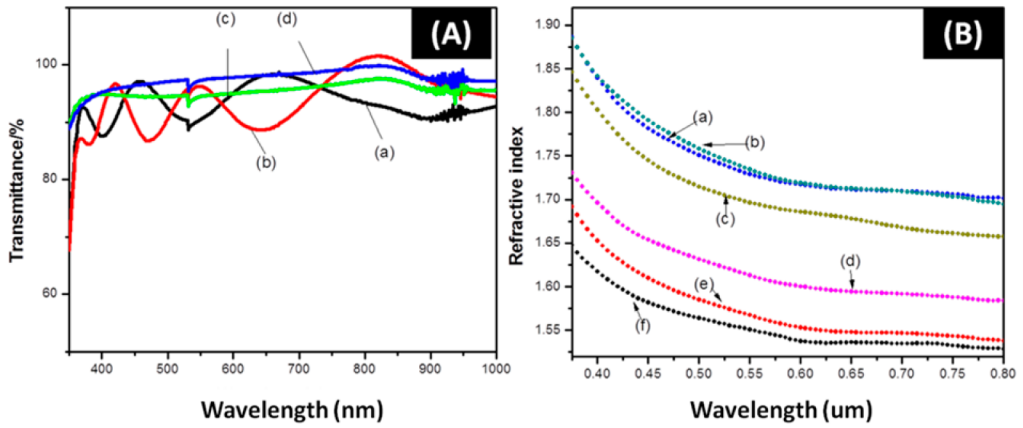

Figure 2. (A) Transmittance of mesoporous TiO_2 nanoparticle films: T90 (a), T80 (b), T70 (c), and T60 (d). (B) Refractive indices of T100 (a), T90 (b), T80 (c), T70 (d), T60 (e), and T50 (f) obtained from ellipsometry.

Table 1. Refractive Index and Porosity of Mesoporous TiO_2 Nanoparticle Films after UV Irradiation

sample	wt % TiO_2 before UV irradiation	refractive index after UV irradiation at 600 nm	porosity (%)
T100	100	1.73	36.1
T90	90	1.72	36.0
T80	80	1.68	39.5
T70	70	1.60	45.3
T60	60	1.55	49.0
T50	50	1.53	51.2

polar protic solvent MeOH. The solvent-exchanged nanoparticles were well-dispersed in the NMP/MeOH mixed solvent [Supporting Information (SI), Figure S1]. The average particle sizes were 8.60 and 8.25 nm before and after solvent exchange, respectively, and the solvent-exchanged dispersion was stable for months.

NOA65 is a UV-curable resin based on thiol-ene click chemistry that consists of trimethylolpropane diallyl ether, trimethylolpropane tris(3-mercaptopropionate), isophorone diisocyanate, and a photonitiator.[39,40] The monomers contain both hydrophilic and hydrophobic groups and can function as molecular surfactants; NOA65 is compatible with TiO_2 nanoparticles in solution without precipitation or aggregation. TiO_2/NOA65 hybrid thin films with different TiO_2 nanoparticle loadings, up to 90 wt %, were obtained by spin-coating. With proper doses of UV radiation, these films were cross-linked into a polymer/nanoparticle network. These thin films were highly transparent in the visible-wavelength range, as confirmed by UV−vis measurements (SI, Figure S2), which

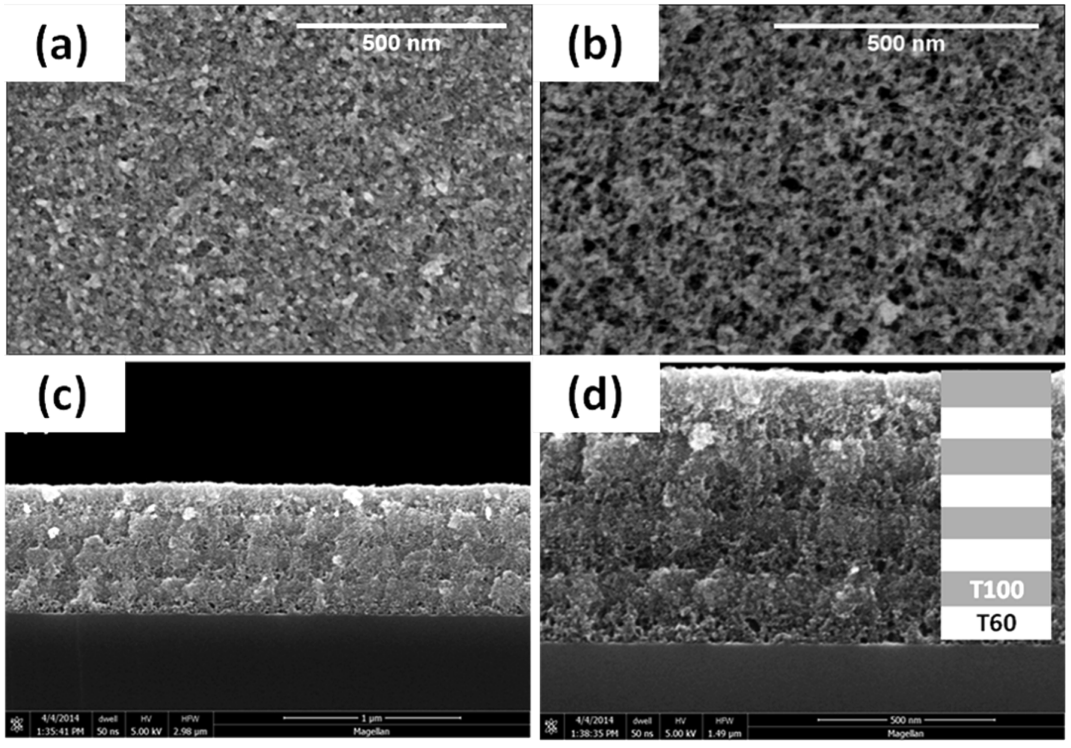

Figure 3. SEM images of the top view of T100 (a) and T60 (b) and cross-sectional images of a Bragg mirror deposited on silicon in different scales (c and d).

DOI: 10.1021/acsami.5b03240
ACS Appl. Mater. Interfaces 2015, 7, 13180−13188

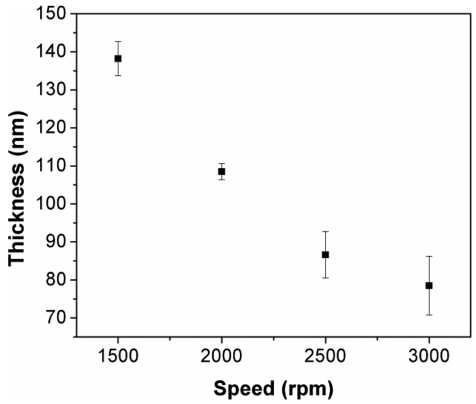

Figure 4. Thicknesses of the T60 layers at different spin-coating speeds as measured by ellipsometry after removal of the template by UV irradiation.

indicated that little TiO_2 nanoparticle aggregation occurred during fabrication. UV curing cross-linked the NOA65 resin, and the resulting hybrid films could not be dissolved in solvents such as MeOH or NMP, allowing additional layers to be spin-coated sequentially on top of one another. UV irradiation was also employed to degrade the organic template to achieve porous TiO_2 films at room temperature. Upon UV exposure, TiO_2 produces holes and electrons that can react with moisture and oxygen in the atmosphere to generate radicals, oxidizing organic components.[33,41] The photoinitiator in NOA65 absorbs UV light around 365 nm to initiate polymerization and TiO_2 absorbs UV light below 350 nm, so initiation of polymerization will not be inhibited by the photoactivity of TiO_2. Because no UV filter was used, polymerization and degradation occurred simultaneously under the UV source. During irradiation, the thickness and refractive index of a hybrid film that contained 60 wt % TiO_2 and 40 wt % NOA65 were monitored via ellipsometry. The films were obtained by spin-coating a 13 wt % solution at 3000 rpm prior to irradiation. As shown in Figure 1a, the film thickness decreased during the first 80 min because of shrinkage from both the polymerization and degradation processes and then remained constant. The refractive index increased after 15 min of irradiation as the resin cross-linked and then began to decrease from 1.77 to 1.74 slowly over 1 h because of degradation of the polymer (Figure 1b). Over the next 1 h, because polymerization was nearly complete, the degradation process dominated and the refractive index decreased 5 times faster than it did in the previous 1 h, stabilizing at 1.55 after 3 h of irradiation. These results indicate that the organic components were completely removed within 3 h of UV irradiation. To determine whether UV light alone could degrade an NOA65 film, a cured NOA65 film was exposed under the same conditions for 3 h. No obvious thickness or refractive index change was observed, which indicated that NOA65 is relatively stable to UV irradiation at these conditions. Therefore, degradation in this TiO_2/NOA65 system is a result of TiO_2 photocatalysis.

IR spectroscopy over the range 4000−650 cm^{-1} was employed to study the UV degradation progress to confirm complete removal of the organic component (SI, Figure S3). The film samples were removed from the substrate and ground into powders for IR characterization. In the spectrum of cured NOA65, a strong absorption centered at 1714 cm^{-1} was characteristic of C═O bond stretching. Peaks at 1235 and 1024 cm^{-1} were assigned to C−O bond stretching in acetate groups. The signal from 2770 to 3360 cm^{-1} resulted from C−H stretching. The broad absorption around 3345 cm^{-1} was assigned to O−H stretching in trimethylolpropane diallyl ether. All of the signals in NOA65 were observed in the IR spectrum of a hybrid composite containing 60 wt % TiO_2 and 40 wt % NOA65 before UV degradation. After UV degradation, all signals from organic components disappeared and the broad

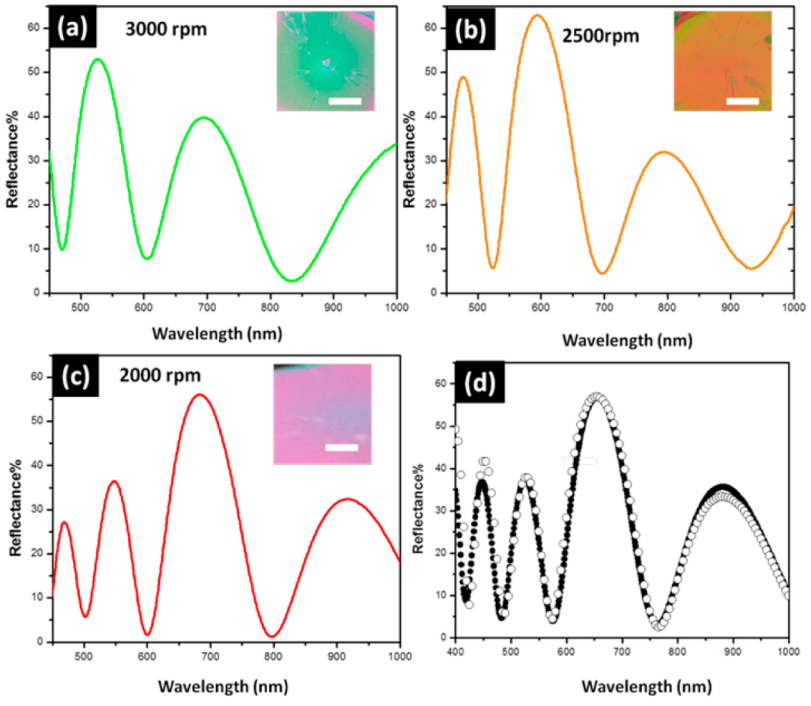

Figure 5. Reflectance of Bragg mirrors indicating colors of green (a), orange (b), and red (c). The scale bar is 500 mm. (d) Experimental (solid) and simulated (circles) data of one Bragg mirror, which is the same sample as that used in the SEM image.

DOI: 10.1021/acsami.5b03240
ACS Appl. Mater. Interfaces 2015, 7, 13180−13188

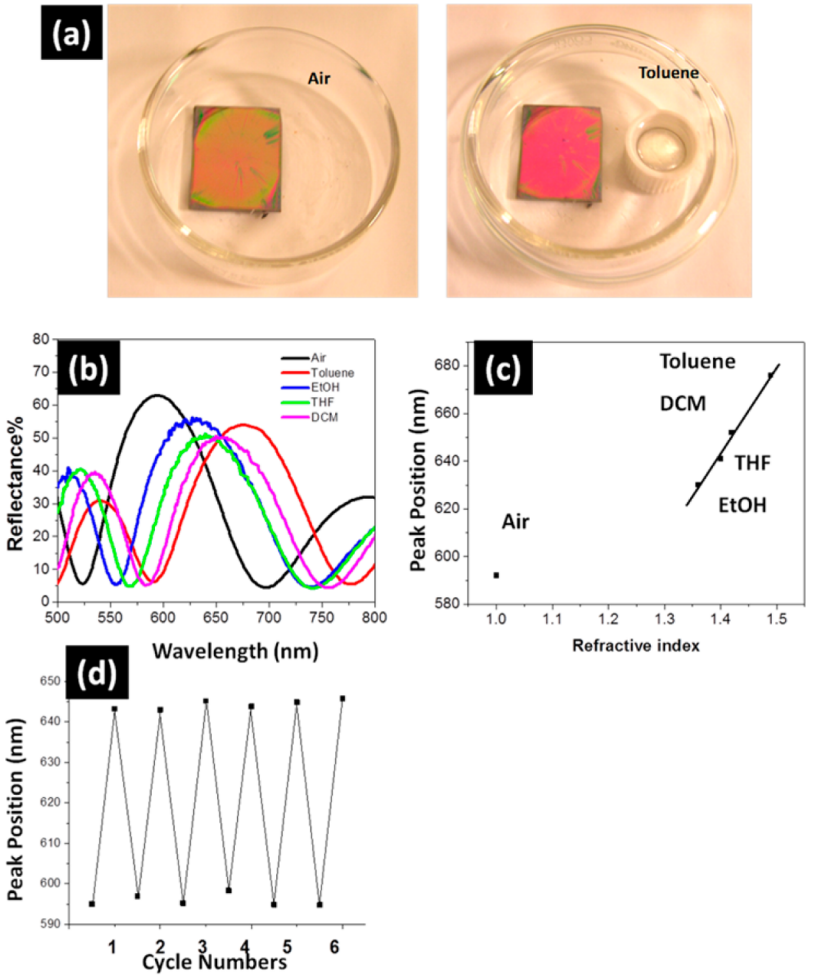

Figure 6. (a) Optical image of a Bragg mirror showing a change in color from orange to red upon exposure to toluene vapor. (b) Reflectance measurements of one Bragg mirror in air and different solvent vapors. (c) Reflectance peak position depending on the refractive index of the solvents. (d) Reflectance peak position of a Bragg mirror in air and toluene vapor over six cycles.

absorption from 3000 to 3300 cm^{-1} was assigned to Ti−OH.[42] The 1634 cm^{-1} peak was assigned to hydroxyl groups in water absorbed on the TiO_2 surface. Strong absorption below 800 cm^{-1} is due to Ti−O−Ti vibration in nanoparticles. These peaks are well-matched with those of pure TiO_2 nanoparticles, indicating that 3 h of radiation with the UV lamp used is sufficient for complete photodegradation of NOA65 at room temperature. In fact, additional experiments show that if the temperature increased to 65 °C when the films were exposed to UV, the complete photodegradation process completed in 1 h (SI, Figure S3d).

Transmittance of the porous 100−400-nm-thick TiO_2 films on glass substrates was characterized using a UV−vis spectrophotometer. The porous TiO_2 films were labeled T60, T70, T80, and T90, where the number indicates the weight percent of TiO_2 nanoparticles in the hybrid films prior to UV degradation. The transmittance measurements show that, after UV degradation, the porous TiO_2 films are highly transparent at all visible wavelengths regardless of the nanoparticle loading (Figure 2A). The high transparency of the films will minimize scattering and absorption losses in each layer, which is important for achieving a high reflection efficiency for the Bragg mirrors.

Refractive indices of TiO_2 hybrid films after UV degradation were measured using VASE[37] (Figure 2B). As shown in Figure 2B, the refractive indices of porous TiO_2 thin films decrease from T90 to T50 because of the greater amount of porosity produced by removing NOA65 from composites containing fewer nanoparticles. Decreasing the TiO_2 loading further below 50 wt % resulted in significant shrinkage during degradation and produced uneven films. A spin-coated 100 wt % TiO_2 nanoparticle film (T100) was also characterized, and it exhibited a refractive index similar to that of T90.

Using the refractive index data, the porosities of mesoporous films can be estimated using the Lorentz−Lorenz relationship.[43] The summarized porosity and refractive index data are shown in Table 1.

Because the porosity of the films is generated from the interstitial space between the TiO_2 nanoparticles, the achievable porosity is limited by jamming of the nanoparticles. Random packing of model identical spheres has been studied for decades, and experimental and simulated results show that the porosity produced by particle jamming has upper and lower limits. The lower limit of the porosity is 36−38% for random close packing,[46] and the upper limit is around 48% for random loose packing.[44,45] In the porous films reported here, spherical nanoparticles were jammed by interactions between themselves and their neighbors. T100 and T90 had porosities around 36%, which is close to the void percent of a random close packing of identical spheres.[46] On the other hand, the porosity of T50 was

DOI: 10.1021/acsami.5b03240
ACS Appl. Mater. Interfaces 2015, 7, 13180−13188

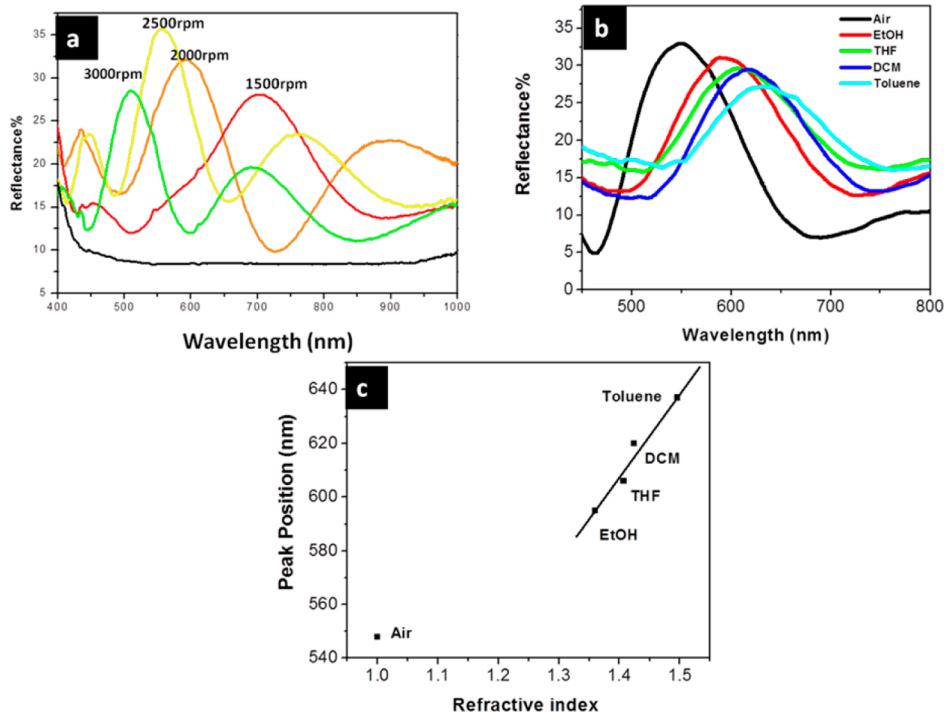

Figure 7. (a) Reflectance measurements of Bragg mirrors with different colors deposited on PET substrates. The numbers above the reflectance peaks indicate the spin-coating speed during fabrication of the T60 layer. (b) Reflectance measurements in air and in different solvent vapors. (c) Reflectance peak shift depending on the refractive indices of the solvents.

around 51%, which is a little bit higher than the upper limit of a random packing of spheres. One explanation for this observation is that the strong interactions between the nanoparticles provided more frictional forces to form a rigid structure to increase the porosity. Indeed, experiments showed that the mesoporous TiO_2 films were stable to heating and sonication for extended periods in common solvents and solvent mixtures including NMP/MeOH, water, isopropyl alcohol, and N,N-dimethylformamide (SI, Table S1). The thicknesses and refractive indices of T60 films did not change after the films were placed in these solvents and sonicated.

The films were relatively stable under mild mechanical force and upon heating. Mesoporous films derived from T60 were sonicated (20 kHz, output energy 1.2 J/s) in water for 30 min or heated on a 150 °C hot plate for 72 h. The thickness and refractive index remained approximately constant before and after these treatments (SI, Figure S4 and Table S1). This indicated that no collapse or particle rearrangement occurred during sonication or heating and that the films were stable under shear and heat. Factors that may stabilize the films include strong interactions between TiO_2 nanoparticles and the UV treatment. UV-light treatment has been shown to improve the interconnection between TiO_2 nanoparticles via the formation of covalent bonds between them.[33,37] One possible mechanism suggested in the literature is that UV-induced oxalation reactions lead to condensation between −OH groups in neighboring TiO_2 nanoparticles.[35]

SEM was employed to study the structure and morphology of the porous TiO_2 thin films. Figure S5 in the SI shows the top view of T100, T90, T80, T70, and T60 thin films. The pore size ranged from 7 to 20 nm, indicating that the films are, in fact, mesoporous.[47] Pore-size distributions were wide, and the structures did not exhibit any long-range order.

The mesoporous TiO_2 nanoparticle films with tunable refractive index are useful building blocks for Bragg mirrors deposited on silicon or PET substrates; T100 and T60 were employed to build Bragg stacks. At 600 nm, the refractive indices of T100 and T60 were 1.73 and 1.53, respectively. A solution containing a 60:40 ratio of TiO_2 to NOA65 was first spin-coated on the substrate. Then the layer was exposed to UV until all of the organic components were degraded, forming the mesoporous TiO_2 film T60. Then a solution containing TiO_2 nanoparticles was spin-coated onto the previously formed mesoporous TiO_2 film to form a T100 layer. These steps were repeated to obtain a Bragg mirror with the target number of layers.

Figure 3 shows SEM images of mesoporous TiO_2 films and a Bragg mirror. All of the samples were studied without further treatment. Parts a and b of Figure 3 show the top views of T100 and T60, respectively, which are the two building block layers, and the difference in the porosity between T100 and T60 is clearly observed. Parts c and d of Figure 3 show the cross-sectional view of a Bragg mirror deposited on silicon. Because the Bragg mirror was made entirely from the same TiO_2 nanoparticles, the contrast between each layer arises only from the porosity difference. The image shows the Bragg mirror structure with eight layers. Cracks are common defects during nanoparticle film fabrication[48,49] and are often observed above a critical crack thickness, which depends on the coating method, solvent, and particle size. However, in this work, no cracking was observed by SEM analysis of our Bragg mirrors deposited on silicon. This could be due to the serial deposition of thin nanoparticle films.[50]

Figure 4 shows the reflectance spectra and optical images of a Bragg mirror deposited on a silicon substrate. To tune the reflectance wavelength, we spin-coated 13 wt % T60 solutions at 3000, 2500, and 2000 rpm to adjust the thickness of the T60

DOI: 10.1021/acsami.5b03240
ACS Appl. Mater. Interfaces 2015, 7, 13180−13188

layers and spin-coated 8.2 wt % T100 solutions at 3000 rpm. The thicknesses of each T60 layer after template removal by UV irradiation are shown in Figure 4, and the thicknesses of T100 were 105.2 ± 3.1 nm, as determined by ellipsometry. Well-defined and thickness-tunable reflectance from green to red wavelengths was demonstrated. As the thickness of the T60 layer increases, the reflectance shifts to longer wavelengths. Secondary reflections are due to Fabry−Perot oscillations generated from the interference between light reflected from the silicon substrate and the top face of the Bragg mirrors. The influence of the layer number on the reflectance was also studied (SI, Figure S6). When the number of bilayers was increased from one to four (one bilayer contains one T60 layer and one T100 layer), the reflectance intensity was increased, while the peak position did not shift significantly. In the porous Bragg mirror fabrication using nanoparticles, the nanoparticles can infiltrate into the pores of the previously deposited layer, which can decrease the porosity and increase the refractive index of each layer because of viscous mass flow at high calcination temperature.[21,29] Here we used simulations to study our Bragg mirrors. *COMSOL Multiphysics* simulation software was employed to build the eight-layer Bragg mirror model. The thicknesses of T60 and T100 were 98 and 103 nm, respectively, which were estimated from the SEM measurement. Refractive index data used in the simulation were obtained from ellipsometry measurements of T60 and T100. Figure 5d shows the simulated results using *COMSOL Multiphysics* simulation software. As Figure 5d shows, the experimental data and simulated results showed a reasonable match for both the intensity and phase. This indicated that the viscous mass flow is inhibited under our room temperature fabrication method. The mesoporous structure is robust, and each layer in the multilayer structure still maintained its original porosity and refractive index, uninfluenced by neighboring layers.

The mesoporous Bragg mirrors can also be used in chemical vapor sensing applications. As Figure 6a shows, the color of one Bragg mirror shifted from orange to red upon exposure to toluene vapor, and the sensor's performance remained stable after several cycles (Figure 6d). This shift of the reflectance of the Bragg mirror indicated that the pores were interconnected within the multilayer structure. The reflectances of Bragg mirrors exposed to other solvent vapors were also measured using a reflectometer equipped with a closed cylinder chamber (3.2 in. diameter and 2.5 in. height). A total of 15 mL of solvent was placed in a vial in the chamber as the solvent vapor source, and the reflectances were recorded after equilibrium. Ethanol (nD^{20} = 1.36), tetrahydrofuran (nD^{20} = 1.40), dichloromethane (nD^{20} = 1.42), and toluene (nD^{20} = 1.50) were employed as test solvents. The peak reflectance shifted to longer wavelengths as the Bragg mirrors were exposed to vapors because of infiltration and condensation of solvent molecules into the pores, and the magnitude of the shift increased with increases in the refractive indices of the solvent vapors. Analysis of the reflectance position suggests a linear relationship between the reflectance wavelength and the refractive index of the solvent vapors, which provides a basis for applications of the mesoporous TiO_2 Bragg mirrors as vapor sensors. The sensitivity of the sensor to the refractive index ($\Delta\lambda/\Delta n$) can be characterized using the slope of the line fit to the data. The slope is 345.2, which indicates that the difference in the peak reflectance wavelength is about 3.4 nm when there is 0.01 refractive index difference between two tested solvent vapors.

Because this method did not require elevated temperatures, it is suitable for the fabrication of Bragg mirrors on flexible PET substrates. However, it is known that PET can be degraded and discolored by extended UV exposure. Here, a control experiment was conducted by exposing a bare PET substrate to the same UV source as that used to fabricate the Bragg mirror. The UV exposure duration was 20 h, which was the same as that used for the fabrication of a 12-layer Bragg mirror. The reflectance and color of the UV-exposed PET did not change significantly after UV exposure, which indicated that this mesoporous TiO_2 fabrication strategy does not influence the optical properties of the PET substrate (SI, Figure S7). Figure S9 in the SI shows an SEM image of the Bragg mirror on PET. No cracks were observed in the film, and the multilayer structure is evident in the SEM image. Figure 7a shows the tunable reflectance of the Bragg mirrors deposited on PET substrates by tuning the spin-coating speed of the T60 layer (the T100 layer was spin-coated at a constant speed of 3000 rpm). When the Bragg mirrors were exposed to different solvent vapors, the reflectance also shifted to longer wavelength and the magnitude of the shift increased with increases of the refractive indices of the solvent vapors, which have the same trend as those deposited on silicon wafers. The sensitivity of the sensor to the refractive index is 325.5, which is close to that of the sensor fabricated on a silicon substrate. The optical properties of the Bragg mirrors after bending were also studied. Figure S8 in the SI indicates that the transmittance profile did not change significantly after a mesoporous TiO_2 Bragg mirror was bent over 100 cycles. The technique reported here could be easily extended to depositing mesoporous TiO_2 Bragg mirrors onto indium−tin oxide (ITO)-coated glass or PET substrates at room temperature, with potential applications in photoelectric devices such as dye-sensitized solar cells.[51]

It should be noted that the refractive indices of the tested solvent vapors are not the only parameters that determine the shift of the reflectance wavelength. The reflectance-wavelength shift also depends on the amount of vapor condensing on the pore surface and within the pore, which is influenced by many factors including as the vapor pressure,[21] environmental humidity,[52] properties of the solvent molecules, and surface energy of the inner pores. In the current study, we mainly focus on the study of a room temperature fabrication method for mesoporous TiO_2 Bragg mirrors, which have shown promise for vapor sensor applications. Quantitative results for single-vapor and mixed-vapor systems can be realized through additional analysis and the use of surface modification to create photonic noses.[23] These efforts are underway.

CONCLUSIONS

We prepared highly transparent TiO_2 hybrid nanocomposite films using commercially available TiO_2 nanoparticles and an NOA65 UV-curable resin. After sufficient UV exposure, the organic binders were degraded via photocatalysis of TiO_2, resulting in mesoporous TiO_2 thin films. This strategy provides a room temperature method to fabricate robust, highly transparent mesoporous TiO_2 films with tunable porosity and refractive index, which are suitable for device fabrication on flexible plastic substrates. By tuning of the TiO_2 to organic binder weight ratio, the refractive indices of the mesoporous films were controlled and the films were used as building blocks for Bragg mirrors. The obtained Bragg mirrors showed well-defined and intense reflectance on both silicon and PET substrates. The applications of mesoporous TiO_2 films with

DOI: 10.1021/acsami.5b03240
ACS Appl. Mater. Interfaces 2015, 7, 13180−13188

tunable porosity include sensors and photoelectric devices. Efforts are underway in characterizing the electrochemical and photoconductive properties of these mesoporous TiO_2 films.

■ ASSOCIATED CONTENT

Supporting Information

Additional characterization such as light scattering, UV−vis, FTIR, ellipsometry, and SEM. The Supporting Information is available free of charge on the ACS Publications website at DOI: 10.1021/acsami.5b03240.

■ AUTHOR INFORMATION

Corresponding Author

*E-mail: watkins@polysci.umass.edu.

Notes

The authors declare no competing financial interest.

■ ACKNOWLEDGMENTS

Funding from the NSF Center for Hierarchical Manufacturing (Grant CMMI-1025020) and G8 Research Councils Initiative on Multilateral Research through the NSF (Grant CMMI-1258336) is gratefully acknowledged. We thank Irene Howell for assistance with the *COMSOL Multiphysics* simulation software.

■ REFERENCES

(1) Keller, U.; Tropper, A. C. Passively modelocked surface-emitting semiconductor lasers. *Phys. Rep.* **2006**, *429*, 67−120.

(2) Choquette, K. D.; Klem, J. F.; Fischer, A. J.; Blum, O.; Allerman, A. A.; Fritz, I. J.; Kurtz, S. R.; Breiland, W. G.; Sieg, R.; Geib, K. M.; Scott, J. W.; Naone, R. L. Room temperature continuous wave InGaAsN quantum well vertical-cavity lasers emitting at 1.3 μm. *Electron. Lett.* **2000**, *36*, 1388−1390.

(3) Hunt, N. E. J.; Schubert, E. F.; Logan, R. A.; Zydzik, G. J. Enhanced spectral power density and reduced linewidth at 1.3 μm in an InGaAsP quantum well resonant-cavity light-emitting diode. *Appl. Phys. Lett.* **1992**, *61*, 2287−2289.

(4) Song, Y.-K.; Diagne, M.; Zhou, H.; Nurmikko, A. V.; Schneider, R. P.; Takeuchi, T. Resonant-cavity InGaN quantum-well blue light-emitting diodes. *Appl. Phys. Lett.* **2000**, *77*, 1744−1746.

(5) Nishimura, S.; Abrams, N.; Lewis, B. A.; Halaoui, L. I.; Mallouk, T. E.; Benkstein, K. D.; van de Lagemaat, J.; Frank, A. J. Standing Wave Enhancement of Red Absorbance and Photocurrent in Dye-Sensitized Titanium Dioxide Photoelectrodes Coupled to Photonic Crystals. *J. Am. Chem. Soc.* **2003**, *125*, 6306−6310.

(6) Lozano, G.; Colodrero, S.; Caulier, O.; Calvo, M. E.; Míguez, H. n. Theoretical Analysis of the Performance of One-Dimensional Photonic Crystal-Based Dye-Sensitized Solar Cells. *J. Phys. Chem. C* **2010**, *114*, 3681−3687.

(7) Shang, G. L.; Fei, G. T.; Zhang, Y.; Yan, P.; Xu, S. H.; Zhang, L. D. Preparation of narrow photonic bandgaps located in the near infrared region and their applications in ethanol gas sensing. *J. Mater. Chem. C* **2013**, *1*, 5285−5291.

(8) Ng, H. M.; Moustakas, T. D.; Chu, S. N. G. High reflectivity and broad bandwidth AlN/GaN distributed Bragg reflectors grown by molecular-beam epitaxy. *Appl. Phys. Lett.* **2000**, *76*, 2818−2820.

(9) Almeida, R. M.; Portal, S. Photonic band gap structures by sol−gel processing. *Curr. Opin. Solid State Mater. Sci.* **2003**, *7*, 151−157.

(10) Almeida, R. M.; Rodrigues, A. S. Photonic bandgap materials and structures by sol−gel processing. *J. Non-Cryst. Solids* **2003**, *326−327*, 405−409.

(11) Chen, K. M.; Sparks, A. W.; Luan, H.-C.; Lim, D. R.; Wada, K.; Kimerling, L. C. SiO_2/TiO_2 omnidirectional reflector and microcavity resonator via the sol−gel method. *Appl. Phys. Lett.* **1999**, *75*, 3805−3807.

(12) Rabaste, S.; Bellessa, J.; Brioude, A.; Bovier, C.; Plenet, J. C.; Brenier, R.; Marty, O.; Mugnier, J.; Dumas, J. Sol−gel fabrication of thick multilayers applied to Bragg reflectors and microcavities. *Thin Solid Films* **2002**, *416*, 242−247.

(13) Kim, E.; Kang, C.; Baek, H.; Hwang, K.; Kwak, D.; Lee, E.; Kang, Y.; Thomas, E. L. Control of Optical Hysteresis in Block Copolymer Photonic Gels: A Step Towards Wet Photonic Memory Films. *Adv. Funct. Mater.* **2010**, *20*, 1728−1732.

(14) Piunova, V. A.; Miyake, G. M.; Daeffler, C. S.; Weitekamp, R. A.; Grubbs, R. H. Highly Ordered Dielectric Mirrors via the Self-Assembly of Dendronized Block Copolymers. *J. Am. Chem. Soc.* **2013**, *135*, 15609−15616.

(15) Sveinbjörnsson, B. R.; Weitekamp, R. A.; Miyake, G. M.; Xia, Y.; Atwater, H. A.; Grubbs, R. H. Rapid self-assembly of brush block copolymers to photonic crystals. *Proc. Natl. Acad. Sci. U. S. A.* **2012**, *109*, 14332−14336.

(16) Choi, S. Y.; Mamak, M.; von Freymann, G.; Chopra, N.; Ozin, G. A. Mesoporous Bragg Stack Color Tunable Sensors. *Nano Lett.* **2006**, *6*, 2456−2461.

(17) Fuertes, M. C.; López-Alcaraz, F. J.; Marchi, M. C.; Troiani, H. E.; Luca, V.; Míguez, H.; Soler-Illia, G. J. A. A. Photonic Crystals from Ordered Mesoporous Thin-Film Functional Building Blocks. *Adv. Funct. Mater.* **2007**, *17*, 1247−1254.

(18) Wang, K.; Morris, M. A.; Holmes, J. D. Preparation of Mesoporous Titania Thin Films with Remarkably High Thermal Stability. *Chem. Mater.* **2005**, *17*, 1269.

(19) Wang, K.; Morris, M. A.; Holmes, J. D. Thermally stable nanocrystallised mesoporous zirconia thin films. *Microporous Mesoporous Mater.* **2009**, *117*, 161.

(20) Wang, K.; Yao, B.; Morris, M. A.; Holmes, J. D. Supercritical Fluid Processing of Thermally Stable Mesoporous Titania Thin Films with Enhanced Photocatalytic Activity. *Chem. Mater.* **2005**, *17*, 4825.

(21) Kobler, J.; Lotsch, B. V.; Ozin, G. A.; Bein, T. Vapor-Sensitive Bragg Mirrors and Optical Isotherms from Mesoporous Nanoparticle Suspensions. *ACS Nano* **2009**, *3*, 1669−1676.

(22) Guldin, S.; Kolle, M.; Stefik, M.; Langford, R.; Eder, D.; Wiesner, U.; Steiner, U. Tunable Mesoporous Bragg Reflectors Based on Block-Copolymer Self-Assembly. *Adv. Mater.* **2011**, *23*, 3664−3668.

(23) Bonifacio, L. D.; Puzzo, D. P.; Breslav, S.; Willey, B. M.; McGeer, A.; Ozin, G. A. Towards the Photonic Nose: A Novel Platform for Molecule and Bacteria Identification. *Adv. Mater.* **2010**, *22*, 1351−1354.

(24) Colodrero, S.; Ocaña, M.; Míguez, H. Nanoparticle-Based One-Dimensional Photonic Crystals. *Langmuir* **2008**, *24*, 4430−4434.

(25) Wu, Z.; Lee, D.; Rubner, M.; Cohen, R. Structural Color in Porous, Superhydrophilic, and Self-Cleaning SiO_2/TiO_2 Bragg Stacks. *Small* **2007**, *3*, 1467−1467.

(26) Smirnov, J. R. C.; Calvo, M. E.; Míguez, H. Selective UV Reflecting Mirrors Based on Nanoparticle Multilayers. *Adv. Funct. Mater.* **2013**, *23*, 2805−2811.

(27) Redel, E.; Mirtchev, P.; Huai, C.; Petrov, S.; Ozin, G. A. Nanoparticle Films and Photonic Crystal Multilayers from Colloidally Stable, Size-Controllable Zinc and Iron Oxide Nanoparticles. *ACS Nano* **2011**, *5*, 2861−2869.

(28) Redel, E.; Mlynarski, J.; Moir, J.; Jelle, A.; Huai, C.; Petrov, S.; Helander, M. G.; Peiris, F. C.; von Freymann, G.; Ozin, G. A. Electrochromic Bragg Mirror: ECBM. *Adv. Mater.* **2012**, *24*, OP265−OP269.

(29) Calvo, M. E.; Colodrero, S.; Rojas, T. C.; Anta, J. A.; Ocaña, M.; Míguez, H. Photoconducting Bragg Mirrors based on TiO_2 Nanoparticle Multilayers. *Adv. Funct. Mater.* **2008**, *18*, 2708−2715.

(30) Colodrero, S.; Mihi, A.; Häggman, L.; Ocaña, M.; Boschloo, G.; Hagfeldt, A.; Míguez, H. Porous One-Dimensional Photonic Crystals Improve the Power-Conversion Efficiency of Dye-Sensitized Solar Cells. *Adv. Mater.* **2009**, *21*, 764−770.

(31) Heiniger, L.-P.; O'Brien, P. G.; Soheilnia, N.; Yang, Y.; Kherani, N. P.; Grätzel, M.; Ozin, G. A.; Tétreault, N. See-Through Dye-

DOI: 10.1021/acsami.5b03240
ACS Appl. Mater. Interfaces 2015, 7, 13180−13188

Sensitized Solar Cells: Photonic Reflectors for Tandem and Building Integrated Photovoltaics. *Adv. Mater.* **2013**, *25*, 5734−5741.
(32) Guldin, S.; Hüttner, S.; Kolle, M.; Welland, M. E.; Müller-Buschbaum, P.; Friend, R. H.; Steiner, U.; Tétreault, N. Dye-Sensitized Solar Cell Based on a Three-Dimensional Photonic Crystal. *Nano Lett.* **2010**, *10*, 2303−2309.
(33) Nakata, K.; Fujishima, A. TiO_2 photocatalysis: Design and applications. *J. Photochem. Photobiol., C* **2012**, *13*, 169−189.
(34) Gutiérrez-Tauste, D.; Zumeta, I.; Vigil, E.; Hernández-Fenollosa, M. A.; Domènech, X.; Ayllón, J. A. New low-temperature preparation method of the TiO_2 porous photoelectrode for dye-sensitized solar cells using UV irradiation. *J. Photochem. Photobiol., A* **2005**, *175*, 165−171.
(35) Tebby, Z.; Babot, O.; Toupance, T.; Park, D.-H.; Campet, G.; Delville, M.-H. Low-Temperature UV-Processing of Nanocrystalline Nanoporous Thin TiO_2 Films: An Original Route toward Plastic Electrochromic Systems. *Chem. Mater.* **2008**, *20*, 7260−7267.
(36) Schröder, M.; Sallard, S.; Böhm, M.; Einert, M.; Suchomski, C.; Smarsly, B. M.; Mutisya, S.; Bertino, M. F. An All Low-Temperature Fabrication of Macroporous, Electrochemically Addressable Anatase Thin Films. *Small* **2014**, *10*, 1566−1574.
(37) Bertino, M. F.; Smarsly, B.; Stocco, A.; Stark, A. Densification of Oxide Nanoparticle Thin Films by Irradiation with Visible Light. *Adv. Funct. Mater.* **2009**, *19*, 1235−1240.
(38) Beaulieu, M. R.; Hendricks, N. R.; Watkins, J. J. Large-Area Printing of Optical Gratings and 3D Photonic Crystals Using Solution-Processable Nanoparticle/Polymer Composites. *ACS Photonics* **2014**, *1*, 799−805.
(39) Benmouna, R.; Benyoucef, B. Thermophysical and thermo-mechanical properties of Norland Optical Adhesives and liquid crystal composites. *J. Appl. Polym. Sci.* **2008**, *108*, 4072−4079.
(40) Nephew, J. B.; Nihei, T. C.; Carter, S. A. Reaction-Induced Phase Separation Dynamics: A Polymer in a Liquid Crystal Solvent. *Phys. Rev. Lett.* **1998**, *80*, 3276−3279.
(41) Thompson, T. L.; Yates, J. T. Surface Science Studies of the Photoactivation of TiO_2 New Photochemical Processes. *Chem. Rev.* **2006**, *106*, 4428−4453.
(42) Lee, L.-H.; Chen, W.-C. High-Refractive-Index Thin Films Prepared from Trialkoxysilane-Capped Poly(methyl methacrylate)−Titania Materials. *Chem. Mater.* **2001**, *13*, 1137−1142.
(43) Hutchinson, N. J.; Coquil, T.; Navid, A.; Pilon, L. Effective optical properties of highly ordered mesoporous thin films. *Thin Solid Films* **2010**, *518*, 2141−2146.
(44) Kamien, R. D.; Liu, A. J. Why is Random Close Packing Reproducible? *Phys. Rev. Lett.* **2007**, *99*, 155501.
(45) Onoda, G. Y.; Liniger, E. G. Random loose packings of uniform spheres and the dilatancy onset. *Phys. Rev. Lett.* **1990**, *64*, 2727−2730.
(46) Torquato, S.; Truskett, T. M.; Debenedetti, P. G. Is Random Close Packing of Spheres Well Defined? *Phys. Rev. Lett.* **2000**, *84*, 2064−2067.
(47) Rouquerol, J.; Avnir, D.; Fairbridge, C. W.; Everett, D. H.; Haynes, J. M.; Pernicone, N.; Ramsay, J. D. F.; Sing, K. S. W.; Unger, K. K. Recommendations for the characterization of porous solids (Technical Report). *Pure Appl. Chem.* **1994**, *66*, 1739.
(48) Lee, W. P.; Routh, A. F. Why Do Drying Films Crack? *Langmuir* **2004**, *20*, 9885−9888.
(49) Dufresne, E. R.; Corwin, E. I.; Greenblatt, N. A.; Ashmore, J.; Wang, D. Y.; Dinsmore, A. D.; Cheng, J. X.; Xie, X. S.; Hutchinson, J. W.; Weitz, D. A. Flow and Fracture in Drying Nanoparticle Suspensions. *Phys. Rev. Lett.* **2003**, *91*, 224501.
(50) Prosser, J. H.; Brugarolas, T.; Lee, S.; Nolte, A. J.; Lee, D. Avoiding Cracks in Nanoparticle Films. *Nano Lett.* **2012**, *12*, 5287−5291.
(51) Park, J. T.; Chi, W. S.; Kim, S. J.; Lee, D.; Kim, J. H. Mesoporous TiO_2 Bragg Stack Templated by Graft Copolymer for Dye-sensitized Solar Cells. *Sci. Rep.* **2014**, *4*, 5505.
(52) Hawkeye, M. M.; Brett, M. J. Optimized Colorimetric Photonic-Crystal Humidity Sensor Fabricated Using Glancing Angle Deposition. *Adv. Funct. Mater.* **2011**, *21*, 3652−3658.

DOI: 10.1021/acsami.5b03240
ACS Appl. Mater. Interfaces 2015, 7, 13180−13188